Vol. 39, No. 4 (2017) 460–470, DOI: 10.24874/ti.2017.39.04.05

Tribology in Industry

www.tribology.fink.rs

RESEARCH

Contact Pressure and Sliding Velocity Maps of the Friction, Wear and Emission from a Low-Metallic/Cast-Iron Disc Brake Contact Pair

J. Wahlström[a], V. Matějka[b], Y. Lyu[a], A. Söderberg[a]

[a]*Department of Machine Design, KTH Royal Institute of Technology, Sweden,*
[b]*Brembo S.p.a., Italy.*

Keywords:

Disc brake
Pin-on-disc
Emissions
Friction
Wear
Maps

Corresponding author:

Jens Wahlström
Department of Machine Design,
KTH Royal Institute of Technology,
Sweden.
E-mail: jensw@kth.se

A B S T R A C T

Particulate matter with an aerodynamic diameter less than 10 μm (PM_{10}) from car disc brakes contribute up to 50% of the total non-exhaust emissions from road transport in the EU. These emissions come from the wear of the pad and rotor contact surfaces. Yet few studies have reported contact pressures and offered sliding speed maps of the friction, wear, and particle emission performance of disc brake materials at a material level. Such maps are crucial to understanding material behaviour at different loads and can be used as input data to numerical simulations. A low-metallic pad and grey cast-iron rotor contact pair commonly used today in passenger car disc brakes was studied using a pin-on-disc tribometer at twelve contact pressure and sliding speed combinations. Maps of the coefficient of friction, specific wear rate, particle number, and mass rate are presented and discussed.

1. INTRODUCTION

In urban areas of the EU the road transport sector contributes up to 64 % [1],[1] of the total particulate matter emissions with an aerodynamic diameter less than 10 μm (PM_{10}). These emissions can be divided into exhaust (tailpipe) and non-exhaust emissions. In the EU, PM_{10} emissions are split about 50/50 between exhaust and non-exhaust emissions [3]. Non-exhaust emissions originate from the wear of brakes, tires, and roads. Resuspension of particles into the air is also considered a source of non-exhaust emission. PM_{10} from disc brakes could contribute up to 50 % of the total non-exhaust emissions from road transport in the EU [4],[5]. Since PM_{10} emissions have adverse health effects [5], the EU has defined European Emission Standards [7] which describe the acceptable limits for exhaust emissions of new vehicles sold in the EU. In the current standard, called EURO6, the exhaust PM limit for petrol and diesel passenger cars is 0.005 g/km. Note that there is no corresponding standard for non-exhaust emissions.

Perricone et al. [8] used a test stand modified for particle emission measurements to determine

emission values for passenger car disc brakes. They showed that for the tested disc brake the PM_{10} emission was around 0.06 g/km, which is the same as the level acceptable under EURO2 set in 1996.

Disc brakes are the most common type of passenger car brakes. Basically, they consist of a calliper with one or more pistons, two pads, and a rotor. During braking, pressure applied inside the calliper makes the piston(s) push the pads into contact with the rotor, which slows the car by transforming kinetic energy into frictional heat. The PM emissions from disc brakes originate from the wear of the pad and rotor contact surfaces. The fact that disc brakes are not sealed from the surroundings is good for cooling, but not good from an emission point of view since the generated wear particles easily leave the system.

The friction, wear, and particle emission performance of the sliding contact pairs in disc brakes can be studied on different scales, ranging from simplified material tests, to component tests with inertia dynamometers [8],[9], to full-scale field tests [8],[10]. Material tests in which the contact pair is replaced by simplified geometries are used to study the material behaviour in a controlled environment without considering the design of the disc brake. These material tests can be used to explain phenomena that occur at the material level and also as a decision tool in the initial phase of the material design process when developing new kinds of brake friction materials.

Pin-on-disc tribometers [12]–[14] are used to conduct material tests of different disc brake material contact pairs. The pin specimens are cut from pad materials while the disc specimens are cut from rotors. The material tests are usually run at constant sliding velocity and normal load, and the outputs are the coefficient of friction and the wear rate. In order to also study particle emissions, the cleanness of the air that surrounds the test specimens needs to be controlled as described by Wahlström et al. [15].

Pin-on-disc tribometer studies of friction, wear, and particle emission dependence on the nominal contact pressure have been reported in the literature for different kinds of disc brake materials [19],[20]. Verma et al. [13] studied friction and wear behaviour with a pin-on-disc tribometer and controlled the disc temperature from 25 to 300 °C with a heating coil. They used one nominal contact pressure and one sliding velocity. None of the above-mentioned studies investigated the friction, wear, and particle emission dependence of both the nominal contact pressure and the sliding velocity, which can be mapped as proposed by Lim and Ashby [15]. These kinds of maps have been shown to be important for numerical simulations of wear [17],[18].

The aim of this study is to map the friction, wear, and particle emission dependence on nominal contact pressure and sliding velocity at a material level using a pin-on-disc tribometer designed for particle emission studies.

2. MATERIALS

The pad and rotor material from the left front disc brake of a typical medium-sized car used in the EU were used in this study (see Fig. 1).
Table **1** shows the data of the reference car and brake system. This disc brake consisted of a sliding calliper, two low-metallic pads, and a ventilated grey cast-iron rotor.

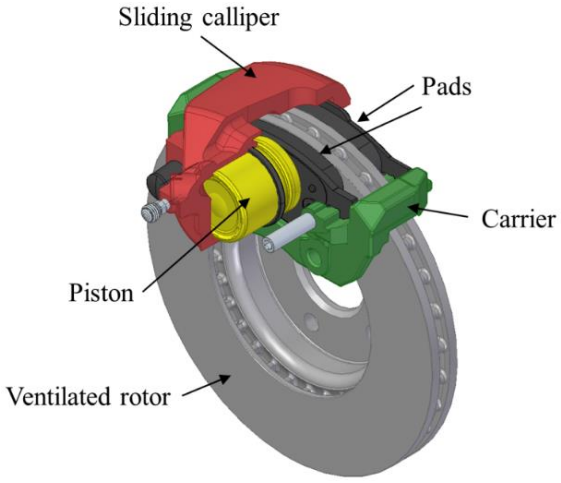

Fig. 1. Single piston sliding calliper disc brake.

Table 1. Data of the car and its front left disc brake.

Front wheel load	690 kg
Wheel radius	314 mm
Rotor outer radius	139 mm
Rotor inner radius	80 mm
Rotor effective radius	113 mm
Pad surface area	5080 mm^2
Cylinder diameter	57 mm

Table 2. Elemental composition of the pad and disc material as measured by X-ray fluorescence spectrometry.

Element	Pin [w%]	Disc [w%]
C	39.8	3.80
Mg	6.50	-
Al	7.11	-
Si	3.13	1.80
S	2.37	0.06
K	1.03	-
Ca	0.52	-
Ti	0.20	-
Cr	2.53	-
Fe	16.7	93.70
Cu	9.12	-
Zn	5.57	-
Mo	0.21	-
Sn	4.08	-
Mn	-	0.65

Cylindrical pin and disc specimens were made from low-metallic pads and cast-iron rotors that are used in the front disc brakes of a medium sized car. The elemental composition measured using X-ray fluorescence spectrometry of the pad friction material and the disc material is shown in Table 2. It reveals a high amount of metallic raw materials (Fe, Cu, Zn). Chromium indicates the presence of chromite. The high amount of magnesium in the presence of (Fe, Mg) with Cr_2O_4 is a widely used abrasive. The high content of magnesium and aluminium also indicates the presence of MgO and Al_2O_3 as abrasives. Sulphur, tin and molybdenum indicate the presence of a solid lubricant based on these three elements. The density of the friction material is 2.75 g/cm^3. The rotor is made of lamellar cast iron with a density of 7100 kg/m^3.

3. PIN-ON-DISC TRIBOMETER

The tests were performed in a pin-on-disc tribometer that has been used for a number of emission studies of disc brake contact pairs in the past [14],[15],[19],[20]. In this setup, the disc specimen is mounted horizontally and is rotated by an electrical motor up to rotational speeds of 3000 rpm. The pin specimen is fixed in a pin holder. Deadweights are used to apply different normal loads from 1 to 100 N on the pin specimen, which results in different nominal contact pressures depending on the nominal contact area. The tangential force is measured using an HBM® Z6FC3/20 kg load cell and the coefficient of friction is determined by dividing this measurement by the applied normal load. The disc temperature was measured with a K-type thermocouple 3 mm below the contact surface.

The mass loss of the test specimens was measured by weighing the test samples before and after the test to the nearest 0.1 mg using a Sartorius® ME614S balance. The specific wear rate for each specimen could then be determined as:

$$k = \frac{\Delta m}{\rho \cdot \Delta s \cdot F_N} \quad (1)$$

where Δm is the mass loss of the specimen, ρ is the density of the specimen, Δs is the sliding distance during the test, and F_N is the normal load applied to the pin. This method enables calculation of the specific wear rate of both pin and disc but it will include the mass losses from running-in.

The tribometer was placed inside a closed box to enable airborne particle measurements. The test equipment is schematically presented in Fig. 2. A fan pumps ambient air through a HEPA filter to the air inlet. The HEPA filter is of class H13 EN 1822 with a collection efficiency of 99.95 % at the maximum penetrating particle size, which ensures particle-free inlet air. The inlet air velocity was measured with a TSI® air velocity transducer model 8455. The air is assumed to be well mixed inside the box due to the complex volume of the pin-on-disc tribometer and the high air exchange rate. The air inside the box transports the generated particles to the air outlet where the sampling point for the particle instruments is located. The temperature and humidity inside the box are measured but they are not controlled.

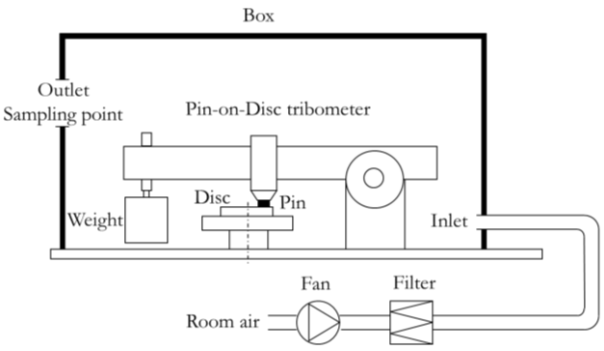

Fig. 2. Schematic image of the test equipment [14].

Three instruments were used to measure particle emissions. The first was a Dekati® Electrical Low-Pressure Impactor (ELPI+) which was used for real-time measurements of particle concentrations for particle diameters from 6 nm up to 10 µm. The second instrument was a TSI® Optical Particle Sizer (OPS) model 3330, which measures particle number concentrations in the size range 0.3 µm to 10 µm. The third instrument was a TSI® Fast Mobility Particle Sizer 3091 (FMPS) spectrometer that measures particle concentrations in the range from 5.6 to 560 nm in 32 channels. The sampling frequency was 1 Hz for all three instruments. The ELPI instrument was used to measure mass concentration while the OPS and FMPS were used to measure number concentrations. With the concentration known, the particle number and mass rates (i.e. the number of particles or mass generated per sliding distance) can be calculated as:

$$n = \frac{1}{s}\int_{t_1}^{t_2} c \cdot Q \cdot dt \tag{2}$$

where c is the measured number or mass concentrations of the particles, Q is the air flow rate through the box, t_1 and t_2 are the start time and end time of the period studied, and s is the sliding distance between t_1 and t_2.

4. DESIGN OF EXPERIMENTS

The tests were conducted with cylindrical pin specimens with diameter 10 mm and disc specimens of 60 mm diameter and 6 mm thickness. The pins were cut from pad friction material and the discs from rotor material.

An inertia dynamometer bench test with the disc brake assembly and the Los Angeles City Traffic (LACT) test cycle showed a mean measured disc temperature of approximately 145 °C and a brake line pressure of approximately 0.7 MPa. The brake line pressure corresponds to a nominal contact pressure of 0.35 MPa. In a previous study by Wahlström et al. [14], pin-on-disc tribometer tests were run with the same kind of materials with a normal load of 47 N and a rotational velocity of 850 rpm that resulted in a disc temperature at steady state of around 154 °C. This is approximately the same as the mean temperature measured during the LACT tests.

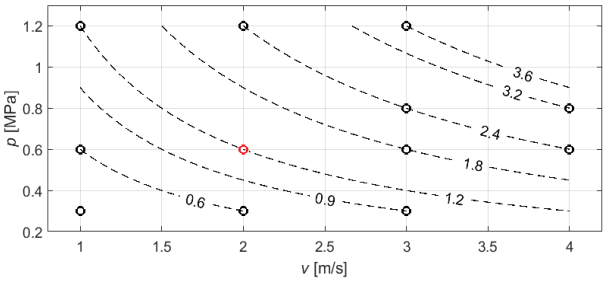

Fig. 3. Nominal contact pressures (p) and sliding velocities (v) used in the pin-on-disc tribometer marked with circles (pv-values [MPa·m/s] are represented with dashed isolines).

The normal load corresponds to a nominal contact pressure of 0.6 MPa and a sliding velocity of 2 m/s. This was used as a basis to capture differences in temperatures that could occur locally during urban driving by choosing contact pressures and sliding velocities around this value. The nominal contact pressures (p) and sliding velocities (v) used in the tests are presented in Fig. 3 with the basis marked by a red circle. The rotational velocity of the disc was set from 425 to 1700 rpm and the nominal contact pressure from 0.3 to 1.2 MPa. The wear track on the disc had a mean diameter of 44 mm resulting in sliding speeds from 1 m/s to 4 m/s. If scaled to the car, the sliding speed corresponds to mean vehicle speeds from 10 to 40 km/h. All tests were run with a sliding distance of about 14.1 km in the middle of the wear track. Three repetitions were run for each test condition. The particle instruments were read to check that there was zero particle concentration inside the box before and after each test was started and stopped.

5. RESULTS

The measured mean coefficient of friction (μ) with plus and minus one standard deviation, mean disc temperatures T_{disc}, mean inlet air speeds (v_{air}), mean particle number (c_{OPS}, c_{FMPS}) and mass concentrations (c_{ELPI}) after run-in are shown in Table 3, along with the weight losses of the pins and discs. Note that for tests 9, 11, and 12, temperature measurements failed since the sliding connection was lost. The values shown were registered directly after the disc rotation was stopped when the connection was resumed. Also note that only one measurement of the temperature was successful in tests 1, 4, 7, and 10 due to failure of the sliding connector for the

thermocouple. The calculated specific wear, particle number, and particle mass rates are shown in Table 4. Note that the particle number rates for the FMPS instrument were not calculated for test conditions 8, 11, and 12 since the standard deviations were the same size as the means. For the same reason, tests 11 and 12 were excluded from the mass rate calculations of the ELPI+ instrument. A coefficient of friction map is presented in Fig. 4. A specific wear rate map for the pin and for the disc is presented in Figs. 5 and 6, respectively. Particle number rate maps as calculated from the OPS and FMPS particle measurements are presented in Fig. 7 and Fig. 8. A particle mass rate map as calculated from the ELPI+ particle instrument is presented in Fig. 9. Note that all the maps are linearly interpolated between the measurement points.

Table 3. Mean, plus and minus one standard deviation, coefficient of friction (μ), disc temperature (T_{disc}), inlet air velocity (v_{air}), pin mass loss (Δm_{pin}), disc mass loss (Δm_{disc}), number concentration as measured by OPS (c_{OPS}) and FMPS (c_{FMPS}), mass concentration as measured by ELPI+ (c_{ELPI}).

Test [#]	p [MPa]	v [m/s]	t [min]	$p \cdot v$ [MPa·m/s]	μ [-]	T_{disc} [°C]	v_{air} [m/s]	Δm_{pin} [mg]	Δm_{disc} [mg]	c_{OPS} [#/cm³]	c_{FMPS} [#/cm³]	c_{ELPI} [mg/m³]
1	0.3	1	240	0.3	0.61 ±0.02	72	0.44 ±0.02	78 ±5	92 ±5	38 ±17	265 ±85	0.10 ±0.03
2	0.3	2	120	0.6	0.53 ±0.02	96 ±6	0.45 ±0.02	51 ±3	25 ±3	88 ±12	730 ±103	0.30 ±0.02
3	0.6	1	240	0.6	0.58 ±0.02	111 ±2	0.42 ±0.01	143 ±3	110 ±5	54 ±12	502 ±147	0.19 ±0.06
4	0.3	3	80	0.9	0.44 ±0.02	125	0.45 ±0.03	26 ±1	16 ±2	73 ±14	356 ±176	0.25 ±0.04
5	0.6	2	120	1.2	0.48 ±0.01	150 ±2	0.46 ±0.004	56 ±4	20 ±1	66 ±4	82 ±10	0.25 ±0.01
6	1.2	1	240	1.2	0.50 ±0.01	165 ±2	0.44 ±0.02	178 ±15	64 ±3	22 ±3	240 ±56	0.09 ±0.02
7	0.6	3	80	1.8	0.47 ±0.01	190	0.44 ±0.03	53 ±3	14 ±4	69 ±4	479 ±207	0.27 ±0.01
8	1.2	2	120	2.4	0.51 ±0.03	260 ±16	0.45 ±0.01	137 ±21	19 ±13	78 ±9	29679 ±29616	1.45 ±1.08
9	0.6	4	60	2.4	0.55 ±0.04	>250	0.43 ±0.01	110 ±38	16 ±4	218 ±42	3100 ±1390	0.80 ±0.15
10	0.8	3	80	2.4	0.52 ±0.03	240	0.46 ±0.001	105 ±23	17 ±4	118 ±18	1482 ±972	0.56 ±0.11
11	0.8	4	60	3.2	0.56 ±0.01	>300	0.38 ±0.01	122 ±11	16 ±2	137 ±51	2229 ±2300	0.51 ±0.23
12	1.2	3	80	3.6	0.60 ±0.01	>300	0.45 ±0.01	217 ±89	23 ±1	128 ±47	170080 ±240000	6.94 ±9.23

Table 4. Calculated specific wear rate of the pin (k_{pin}) and disc (k_{disc}), particle number rate (n_{OPS} and n_{FMPS}), and particle mass rate (n_{ELPI}).

Test [#]	p [MPa]	v [m/s]	$p \cdot v$ [MPa·m/s]	k_{pin} [10^{-14}m³/Nm]	k_{disc} [10^{-15}m³/Nm]	n_{OPS} [#/m]	n_{FMPS} [#/m]	n_{ELPI} [µg/m]
1	0.3	1	0.3	7.8	36.6	80508	562977	0.22
2	0.3	2	0.6	5.0	9.9	94459	784325	0.32
3	0.6	1	0.6	7.6	23.5	113655	1050317	0.40
4	0.3	3	0.9	2.6	6.4	52359	255566	0.18
5	0.6	2	1.2	3.0	4.2	72032	88845	0.28
6	1.2	1	1.2	4.9	7.1	46901	507173	0.20
7	0.6	3	1.8	2.8	2.9	48301	336551	0.19
8	1.2	2	2.4	3.8	2.1	84182	-	-
9	0.6	4	2.4	5.8	3.4	113390	1608928	0.42
10	0.8	3	2.4	4.2	2.8	85770	1076298	0.40
11	0.8	4	3.2	4.9	2.5	62160	-	0.23
12	1.2	3	3.6	6.0	2.5	92851	-	-

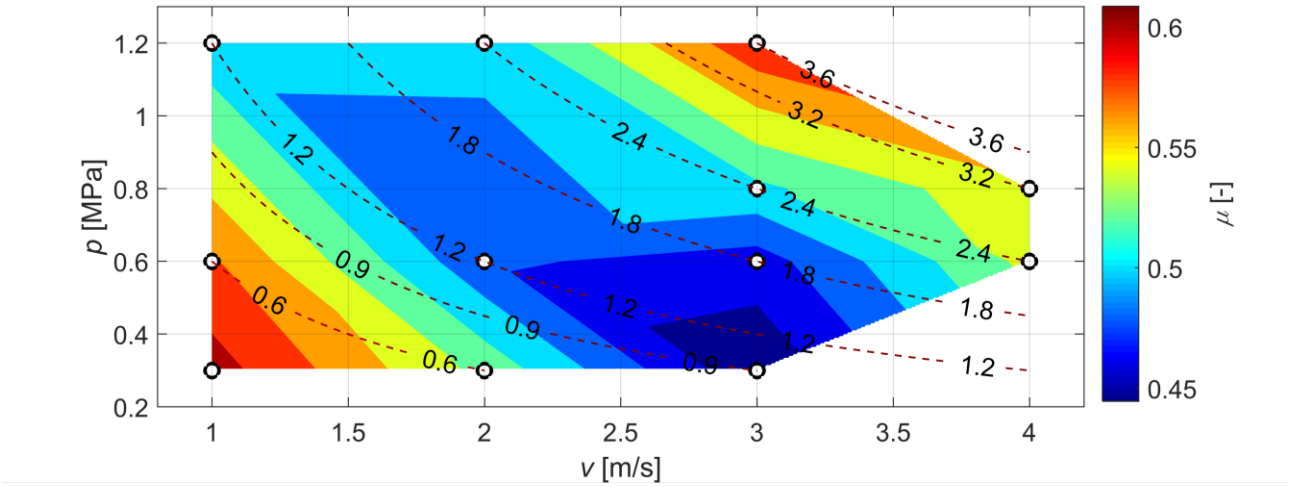

Fig. 4. Contact pressure and sliding velocity map of the coefficient of friction.

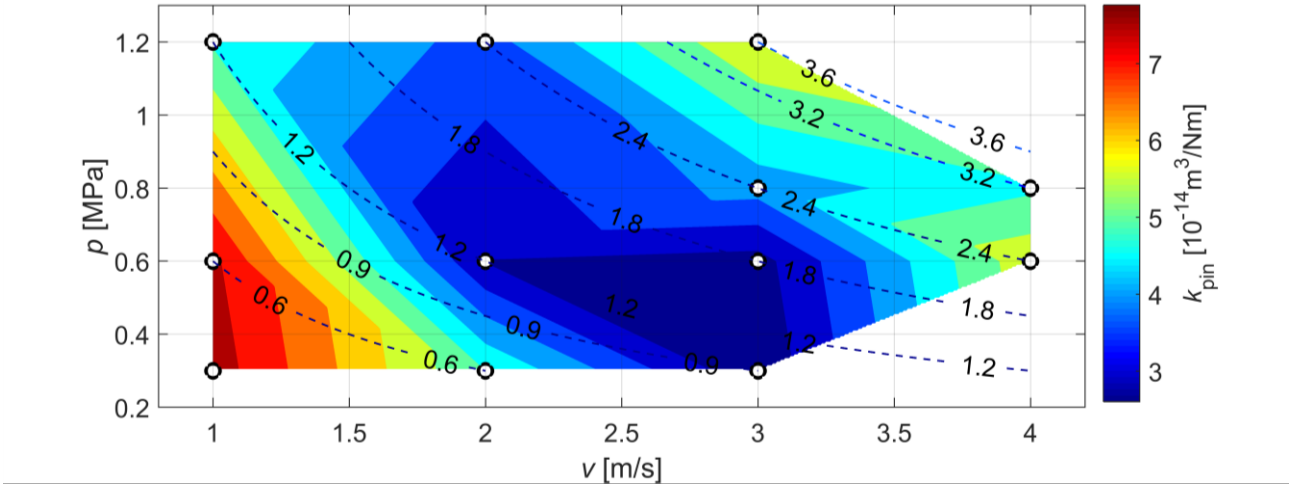

Fig. 5. Contact pressure and sliding velocity map of the specific wear rate of the pin friction material.

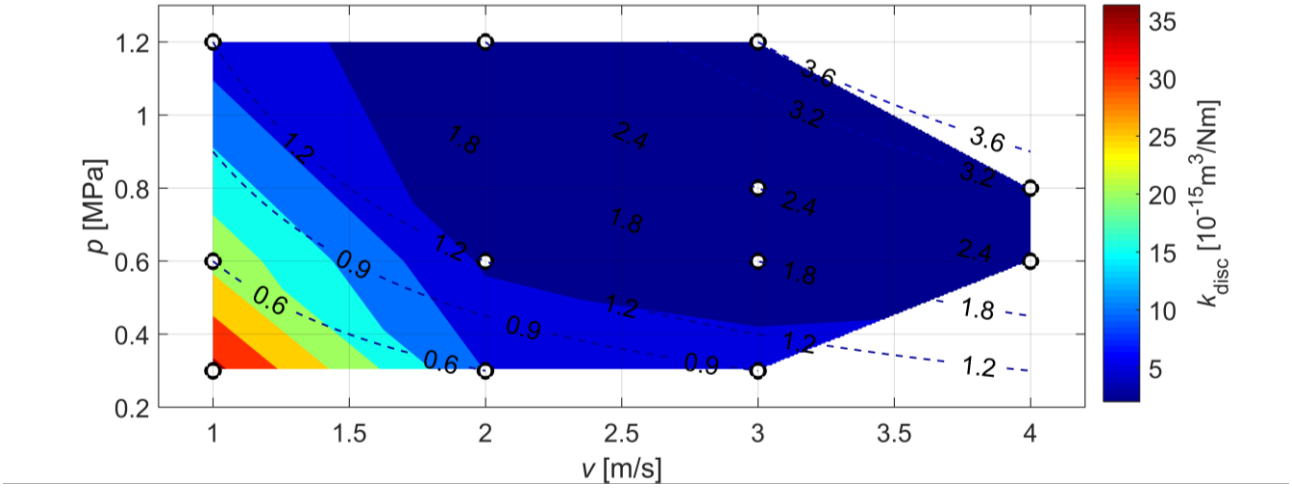

Fig. 6. Contact pressure and sliding velocity map of the specific wear rate of the disc (pv-values [MPa·m/s] are represented with dashed isolines).

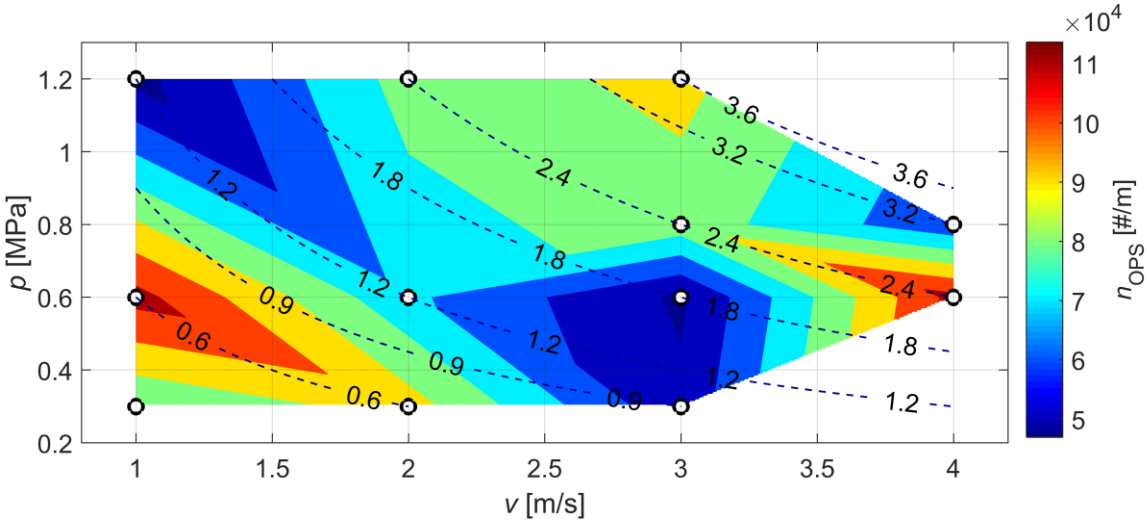

Fig. 7. Contact pressure and sliding velocity map of the number rate calculated from the OPS instrument (pv-values [MPa·m/s] are represented with dashed isolines).

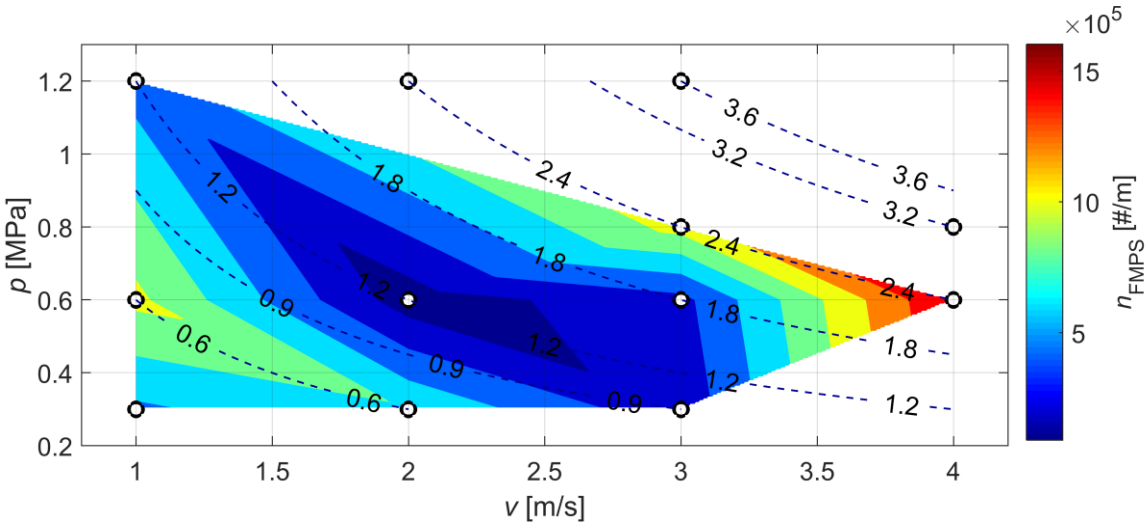

Fig. 8. Contact pressure and sliding velocity map of the particle number rate calculated from the FMPS instrument (pv-values [MPa·m/s] are represented with dashed isolines).

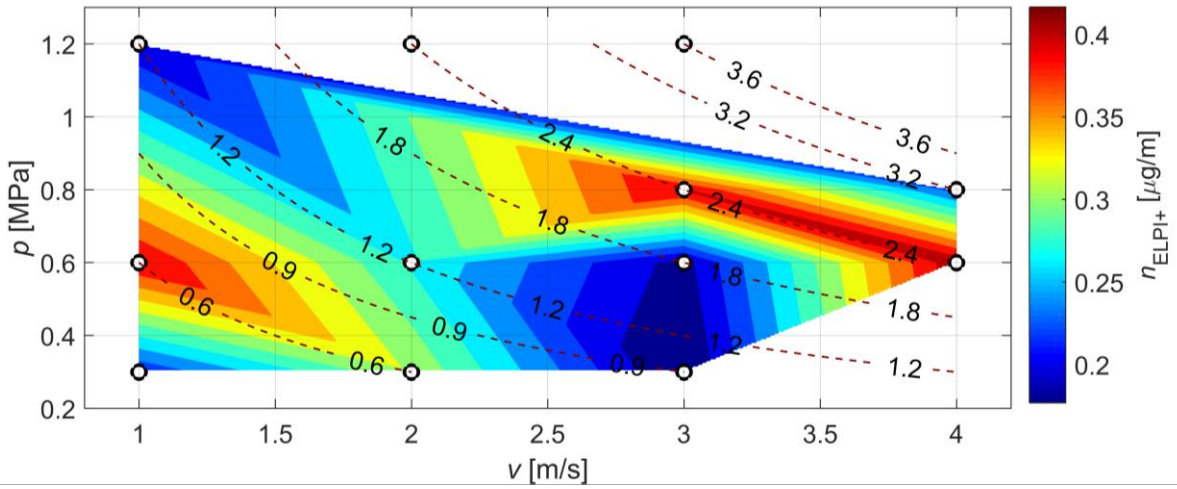

Fig. 9. Contact pressure and sliding velocity map of the particle mass rate calculated from the ELPI+ instrument (pv-values [MPa·m/s] are represented with dashed isolines).

6. DISCUSSION

As can be seen in Fig. 4 and Table 3, the coefficient of friction first decreases and then increases with increasing pv value and disc temperature. The frictional, wear, and particle emission behaviour of disc brakes will be explained in terms of different size scales.

The macroscopic wear behaviour of disc brakes is explained by the mesoscopic contact situation between the pad and disc [21],[22]. Metal fibres in the pad form stable primary plateaus that carry the main part of the load. Wear particles are transported in the boundary layer between the pad and the disc. Some wear particles stack up against the primary plateaus and create secondary plateaus. The mesoscopic contact situation has been numerically simulated and validated by tests conducted in an inertia dynamometer bench by Wahlström [23]. On the microscopic scale, Österle et al. [24],[24] observed that the friction is determined by the shearing of a 100 nm thick nanocrystalline tribofilm that covers both the contact surfaces. This tribofilm is formed by a combination of plastic deformation, compaction, oxidation, and mechanical mixing of wear particles. Furthermore, Österle et al. concluded that the tribofilm consists mainly of iron oxides with a grain size of approximately 10–100 nm. Österle et al. [26] also conducted numerical simulations of this tribofilm on a microscopic scale and concluded that the coefficient of friction decreases with increasing pressure since the thickness of the tribofilm increases and is easier to shear. Since the coefficient of friction depends on the contact pressure, which in turn is dependent on the contact area, the microscopic and mesoscopic behaviours are both dependent on wear. The amount of wear needs to be enough to create secondary plateaus that will increase the contact area and decrease the contact pressure. With decreased contact pressure, the tribofilm will be thinner and the coefficient of friction will increase. This dependence of the coefficient of friction on contact pressure is in line with the results presented in Fig. 4 for the lowest sliding velocity. It has also been observed by Wahlström [27] who used a numerical factorial design to study the effects of the properties of brake pad friction material on friction and wear emissions.

Figure 4 also shows that the coefficient of friction decreases with increasing sliding velocity. This could be explained by the increased contact area because of higher wear. The combination of plateau dynamics and the impact of the tribofilm on the coefficient of friction possibly explain the measured coefficient of friction up to the pv value of 2 MPa·m/s and a disc temperature around 200 °C. This temperature has also been reported by Alemani et al. [20]. Above this value it seems the wear of the resin takes over since the temperature of the pad resin is probably high enough to start degrading. This could explain why the resin of the friction material wears up to ten times faster [28] than at moderate temperatures. In turn, this could lead to the secondary plateaus breaking down and the contact pressure increasing. The coefficient of friction will then go down, as can be seen in Fig. 4. This behaviour has also been reported by Verma et al. [13].

The degradation of the resin also creates a large number of ultrafine airborne particles [19],[20],[29] as can be seen in Table 3 (test 12) for the FMPS instrument. The increased specific wear rate of the pin can also be seen for test 12. This strengthens the hypothesis that this is a temperature dependent phenomenon on the pin surface. The specific wear rate of the disc seems to be quite stable above a certain specific power and is not affected by increasing temperature.

The pv maps could be used in the initial friction material design phase to understand how a novel material behaves at different load conditions. As can be seen in Figs. 4–9, it seems preferable for the contact pair to work at a pv number of about 1.8 MPa·m/s since that is where the specific wear rate of the pin friction material, the particle number, and mass rates have the lowest values. Also, the coefficient of friction is relatively stable around this value, and the specific wear rate of the disc is low. These results are important input data for brake designers since they provide initial values for the braking pressures and sliding velocities at which the disc brake should work.

The friction, wear, and particle emission of the full pad to rotor contact pair depends on the contact conditions, which in turn depend on the design of the disc brake system. The contact

conditions depend on several variables such as the contact pressure distribution, real contact area, sliding velocity, contact temperature distribution, materials, surface geometry, and surface hardness. These variables cannot be regarded as constant during a typical braking event. That is, the contact conditions will change both in time and space during braking. The normal load acting on the back of the pad and the rotational speed of the disc could be controlled during testing, and from these a nominal contact pressure, nominal contact area, and sliding speed can be determined.

It is difficult to study how the contact pressure distribution and real contact area change during a brake event by conducting experiments. Some experiments reported in the literature [30],[31] used a disc made of glass to see what is going on in the contact, but the friction influence of the disc is lost. Finite element analysis (FEA) at the macroscopic scale could be used to better understand how the contact pressure is distributed in the contact during braking [31],[33],[34]. To be able to simulate friction, wear, and particle emissions, the local coefficient of friction, specific wear rate, and particle number rate depending on local contact pressure and sliding velocity need to be known. One FEA approach would be to divide the pad into a number of pins, each with a local contact pressure and sliding velocity determined by using maps like those presented in this paper.

It should be noted that the disc in the experiment rotates in the horizontal plane while the brake rotor rotates in the vertical plane. This could affect the creation of plateaus as wear debris could travel with the disc back into the contact. Also note that the heat partition between the specimens in the current test setup does not correspond to what can be observed in dynamometer bench tests.

The friction, wear, and particle emission can be determined with the pin-on-disc tribometer setup on the assumption that the contact conditions in the pin-on-disc tribometer represent the contact conditions at the pad to rotor interface. Metinoz et al. [35] compared pad and rotor surfaces after an inertia dynamometer bench test with pin and disc surfaces after a pin-on-disc tribometer test. They concluded that although the test setups were very different, the results show that tribometers provide information related to the friction-wear performance, character of friction surfaces, and character of wear particles, which reflect the behaviour of the samples during dynamometer bench tests.

To be able to model the particle emissions, it is important to have a reliable estimation of the number and mass rate of the particles. It is not clear that such estimates can be obtained with the current test set up. As can be seen in Table 3, the generation of particles is very unsteady at the highest temperatures, and the repeatability of the tests is very low. One explanation is that the temperature of the aerosol sampled is not controlled, which may lead to thermally unstable volatiles being counted by the particle instruments. A solution is to use a volatile particle remover (VPR) to remove the volatiles before the aerosol is sampled, as is done in exhaust measurements [7]. Furthermore, the sampling of the aerosol is anisokinetic, which could mean that that the measured sample concentrations are not representative of the particles generated in the chamber. This issue can be addressed by re-designing the chamber to allow isokinetic particle sampling as discussed by Riva et al. [35].

7. CONCLUSION

The friction, wear, and particle emission dependence of nominal contact pressure and sliding velocity for a typical disc brake contact pair have been mapped using a pin-on-disc tribometer. The following conclusions can be drawn from this study:

- The coefficient of friction and the specific wear rate of the pin decrease with increasing contact pressure and sliding velocity until the disc temperature reaches about 200 °C; thereafter they increase.
- The specific wear rate of the disc decreases with increasing contact pressure and sliding velocity.
- The particle mass and number rates seem to decrease with increasing contact pressure and sliding velocity until the disc temperature is about 200 °C; thereafter they increase.

The repeatability of the particle measurements at disc temperatures above 200 °C is questionable. The particle sampling setup should be redesigned to allow isokinetic sampling and removal of volatiles.

Acknowledgement

The research leading to these results received funding from the European Union's Horizon 2020 research and innovation programme under grant agreement No. 636592 (LOWBRASYS project).

REFERENCES

[1] P. Pant and R.M. Harrison, 'Estimation of the contribution of road traffic emissions to particulate matter concentrations from field measurements: A review', *Atmospheric Environment*, vol. 77, pp. 78–97, 2013.

[2] A. Suleiman, M.R. Tight and A.D. Quinn, 'Assessment and prediction of the impact of road transport on ambient concentrations of particulate matter PM10', *Transportation Research. Part D: Transport and Environment*, vol. 49, pp. 301–312, 2016.

[3] C. Hak, S. Larssen, S. Randall, C. Guerreiro, B. Denby and J. Horálek, 'Traffic and air quality contribution of traffic to urban air quality in European cities', *ETC/ACC*, Technical Paper 2009/12, 2009.

[4] T. Grigoratos and G. Martini. 'Brake wear particle emissions: A review', *Environmental Science and Pollution Research*, vol. 22, pp. 2491–2504, 2015.

[5] R.M. Harrison, A.M. Jones, J. Gietl, J. Yin and D.C. Green, 'Estimation of the contributions of brake dust, tire wear, and resuspension to nonexhaust traffic particles derived from atmospheric measurements', *Environmental Science & Technology*, vol. 46, pp. 6523–6529, 2012.

[6] M. Gasser, M. Riediker, L. Mueller, A. Perrenoud, F. Blank, P. Gehr and B. Rothen-Rutishauser, 'Toxic effects of brake wear particles on epithelial lung cells in vitro', *Particle and Fibre Toxicology*, vol. 6, 2009. doi: 10.1186/1743-8977-6-30.

[7] European Commission. Commission Regulation (EU) No 459/2012 of 29 May 2012.

[8] M. Alemani. Particle emissions from car disc brakes: the influence of contact conditions on the pad-to-rotor interface. Doctoral Thesis. KTH Royal Institute of Technology. ISBN: 978-91-7729-462-7.

[9] G. Perricone, J. Wahlström and U. Olofsson. 'Towards a test stand for standardized measurements of the brake emissions', *Proceedings of the Institution of Mechanical Engineers. Part D: Journal of Automobile Engineering*, vol. 230, pp. 1521–1528, 2016.

[10] G. Perricone, M. Alemani, I. Metinöz, V. Matějka, J. Wahlström and U. Olofsson, 'Towards the ranking of airborne particle emissions from car brakes: A system approach', *Proceedings of the Institution of Mechanical Engineers. Part D: Journal of Automobile Engineering*, vol. 231, pp. 781–797, 2017.

[11] J. Wahlström and U. Olofsson, 'A field study of airborne particle emissions from automotive disc brakes', *Proceedings of the Institution of Mechanical Engineers. Part D: Journal of Automobile Engineering*, vol. 229, pp. 747–757, 2015.

[12] J. Wahlström, A. Söderberg, L. Olander U. Olofsson and A. Jansson, 'A pin-on-disc simulation of airborne wear particles from disc brakes', *Wear*, vol. 268, pp. 763–769, 2010.

[13] P.C. Verma, R. Ciudin, A. Bonfanti, P. Aswath, G. Straffelini and S. Gialanella, 'Role of the friction layer in the high-temperature pin-on-disc study of a brake material', *Wear*, vol. 346–347, pp. 56–65, 2016.

[14] J. Wahlström, Y. Lyu, V. Matějka and A. Söderberg, 'A pin-on-disc tribometer study of disc brake contact pairs with respect to wear and airborne particle emissions', *Wear*, vol. 384–385, pp. 124–130, 2017.

[15] J. Wahlström, D. Gventsadze, L. Olander, E. Kutelia, L. Gventsadze, O. Tsurtsumia and U. Olofsson, 'A pin-on-disc investigation of novel nanoporous composite-based and conventional brake pad materials focussing on airborne wear particles'. *Tribology International*, vol. 42, pp. 1838–1843, 2011.

[16] S.C. Lim and M.F. Ashby, 'Wear-mechanism maps', *Scripta Metallurgica et Materialia*, vol. 35, pp. 1–24, 1987.

[17] R. Enblom and M. Berg, 'Simulation of railway wheel profile development due to wear: Influence of disc braking and contact environment', *Wear*, vol. 258, pp. 1055–1063, 2005.

[18] A. Rovira, A. Roda, M.B. Marshall, H. Brunskill and R. Lewis, 'Experimental and numerical modelling of wheel–rail contact and wear', *Wear*, vol. 271, pp. 911–924, 2011.

[19] J. Wahlström, L. Olander and U. Olofsson, 'A pin-on-disc study focusing on how different load

levels affect the concentration and size distribution of airborne wear particles from the disc brake materials', *Tribology Letters*, vol. 46, pp. 195–204, 2012.

[20] M. Alemani, U. Olofsson, G. Perricone, A. Söderberg, J. Wahlström and A. Ciotti, 'A study on the load level influence on particulate matter emissions from the sliding contact between a low steel friction material and cast iron', in *Eurobrake 2015,* Dredsen, Germany 4–6 May 2015.

[21] M. Eriksson, F. Bergman and S. Jacobson, 'On the nature of tribological contact in automotive brakes', *Wear*, vol. 252, pp. 26–36, 2002.

[22] W. Österle, M. Griepentorg, T. Gross and I. Urban, 'Chemical and microstructural changes induced by friction and wear of brakes', *Wear*, vol. 251, pp. 1469–1476, 2001.

[23] J. Wahlström, 'A comparison of measured and simulated friction, wear, and particle emission of disc brakes', *Tribology International*, vol. 92, pp. 503-511, 2015.

[24] W. Österle and I. Urban, 'Friction layers and friction films on PMC brake pads', *Wear*, vol. 257, pp. 215–226, 2004.

[25] W. Österle and I. Urban, 'Third body formation on brake pads and rotors', *Tribology International*, vol. 39, pp. 401–408, 2006.

[26] W. Österle and A.I. Dmitriev, 'Functionality of conventional brake friction materials: Perceptions from findings observed at different length scales', *Wear*, vol. 271, pp. 2198–2207, 2011.

[27] J. Wahlström, 'A Factorial Design to Numerically Study the Effects of Brake Pad Properties on Friction and Wear Emissions', *Advances in Tribology*, vol. 2016, Article ID 8181260, 2016.

[28] A.L. Cristol-Bulthé, Y. Desplanques, G. Degallaix and Y. Berthier, 'Mechanical and chemical investigation of the temperature influence on the tribological mechanisms occurring in OMC/cast iron friction contact', *Wear*, vol. 264, pp. 815–825, 2008.

[29] J. Kukutschová, P. Moravec, V. Tomášek, V. Matějka, J. Smolík, J. Schwarz, J. Seidlerová and K. Šafářová, P. Filip, 'On airborne nano/micro-sized wear particles released from low-metallic automotive brakes', *Environmental Pollution*, vol. 159, pp. 998–1006, 2011.

[30] M. Eriksson, J. Lord and S. Jacobson, 'Wear and contact conditions of brake pads: dynamical in situ studies of pad on glass', *Wear*, vol. 249, pp. 272–278, 2001.

[31] S. Gramstadt, 'Methoden der in-situ Visualisierung der Reibzonendynamik trockenlaufender Reibpaarungen unter Ergänzung physikalischer und chemischer Charakterisierungen der Reibpartner', *Doctoral thesis*. Universitätsverlag Ilmenau, Ilmenau, Germany, ISBN 978-3-86360-107-2, 2015.

[32] M. Tirovic and A.J. Day, 'Disc brake interface pressure distributions', *Proceedings of the Institution of Mechanical Engineers. Part D: Journal of Automobile Engineering*, vol. 205, pp. 137–146, 1991.

[33] A. Söderberg and S. Andersson, 'Simulation of wear and contact pressure distribution at the pad-to-rotor interface in a disc brake using general purpose finite element analysis software', *Wear*, vol. 267, pp. 2243–2251, 2009.

[34] J. Wahlström, A. Söderberg and U. Olofsson, 'Simulation of airborne particles from disc brakes', *SAE Technical Paper*: 2009-01-3040, 2009.

[35] I. Metinöz, V. Matějka, M. Alemani, J. Wahlström and G. Perricone, 'Could pin-on-disc tribometers be used to study the friction/wear performance of disc brake materials?', in *Eurobrake 2016*, Milano, Italy 13–15 June 2016.

[36] G. Riva, J. Wahlström, M. Alemani and U. Olofsson, 'A CFD study of a pin-on-disc tribometer setup focusing on airborne particle sampling efficiency', in *Ecotrib 2017*, Ljubljana, Slovenia 7–9 June 2017.